Journal of Hydrology 381 (2010) 352–363

Contents lists available at ScienceDirect

Journal of Hydrology

journal homepage: www.elsevier.com/locate/jhydrol

El-Niño/Southern Oscillation (ENSO) influences on monthly NO_3 load and concentration, stream flow and precipitation in the Little River Watershed, Tifton, Georgia (GA)

V.W. Keener [a,*], G.W. Feyereisen [b], U. Lall [c], J.W. Jones [a], D.D. Bosch [d], R. Lowrance [d]

[a] Department of Agricultural and Biological Engineering, University of Florida, Gainesville, FL 32601, USA
[b] USDA-ARS-Pasture Systems & Watershed Mgt. Research Unit, University Park, PA 16802, USA
[c] Department of Earth and Environmental Engineering, Columbia University, New York, NY, USA
[d] USDA-ARS-Southeast Watershed Research Laboratory, 2375 Rainwater Road, Tifton, GA 31794, USA

ARTICLE INFO

Article history:
Received 10 March 2009
Received in revised form 3 December 2009
Accepted 3 December 2009

This manuscript was handled by K. Georgakakos, Editor-in-Chief, with the assistance of A.A. Tsonis, Associate Editor

Keywords:
ENSO
El Niño
Wavelets
Nutrients
Hydrology
Southeast US

SUMMARY

As climate variability increases, it is becoming increasingly critical to find predictable patterns that can still be identified despite overall uncertainty. The El-Niño/Southern Oscillation is the best known pattern. Its global effects on weather, hydrology, ecology and human health have been well documented. Climate variability manifested through ENSO has strong effects in the southeast United States, seen in precipitation and stream flow data. However, climate variability may also affect water quality in nutrient concentrations and loads, and have impacts on ecosystems, health, and food availability in the southeast. In this research, we establish a teleconnection between ENSO and the Little River Watershed (LRW), GA., as seen in a shared 3–7 year mode of variability for precipitation, stream flow, and nutrient load time series. Univariate wavelet analysis of the NINO 3.4 index of sea surface temperature (SST) and of precipitation, stream flow, NO_3 concentration and load time series from the watershed was used to identify common signals. Shared 3–7 year modes of variability were seen in all variables, most strongly in precipitation, stream flow and nutrient load in strong El Niño years. The significance of shared 3–7 year periodicity over red noise with 95% confidence in SST and precipitation, stream flow, and NO_3 load time series was confirmed through cross-wavelet and wavelet-coherence transforms, in which common high power and co-variance were computed for each set of data. The strongest 3–7 year shared power was seen in SST and stream flow data, while the strongest co-variance was seen in SST and NO_3 load data. The strongest cross-correlation was seen as a positive value between the NINO 3.4 and NO_3 load with a three-month lag. The teleconnection seen in the LRW between the NINO 3.4 index and precipitation, stream flow, and NO_3 load can be utilized in a model to predict monthly nutrient loads based on short-term climate variability, facilitating management in high risk seasons.

© 2009 Elsevier B.V. All rights reserved.

Introduction

Climate variability and change are areas of high priority research both locally and globally. Recent research has shown that extremes of climate such as heat waves, droughts, floods and tropical cyclones may be becoming more common (IPCC, 2007). Climate variability directly affects a range of hydrological variables, such as precipitation and water quantity. By extension, climate variability also may affect water quality as seen in pollutants, although these concerns are often overlooked in favor of focusing on stream flow amounts and timing. However, volumes of stream flow may not be the most important factor if water quality is lowered to a point where the utility in natural or manmade ecosystems is compromised. There is a need to identify climate non-stationarities and their links to watershed outcomes. In particular, for risk management, inter-annual modes of climate variability and their seasonal expression are of interest. The specific contribution of this paper is that it is one of the first analyses to link water quality parameters to these non-stationary climate modes. The recent IPCC technical paper 'Climate Change and Water' suggests with high confidence that the increase in global climate variability and extremes may exacerbate some types of water pollution, leading to declines in water quality that could affect food availability, human health, water infrastructure operating costs, and ecosystem health (Bates et al., 2008). This research is targeted at exploring the relationship between climate variability at the inter-annual level via the El-Niño/Southern Oscillation (ENSO) and hydrology and

* Corresponding author. Tel.: +1 352 392 1864x288; fax: +1 352 392 4092.
E-mail addresses: vicko@ufl.edu (V.W. Keener), Gary.Feyereisen@ars.usda.gov (G.W. Feyereisen), ula2@columbia.edu (U. Lall), jimj@ufl.edu (J.W. Jones), David.Bosch@ars.usda.gov (D.D. Bosch), Richard.Lowrance@ars.usda.gov (R. Lowrance).

0022-1694/$ - see front matter © 2009 Elsevier B.V. All rights reserved.
doi:10.1016/j.jhydrol.2009.12.008

water quality at the small basin scale in the Little River Watershed, Georgia (GA). By quantifying the relationships between inter-annual climate and water quality, it may be possible to use this information to reduce pollutant loads into target watersheds during high risk months using short-term climate predictions.

The ENSO is a periodic ocean and atmospheric phenomenon with strong effects on the climate of the southeast United States. The tri-state region especially, Florida, GA, and Alabama, experiences strong ENSO effects. El Niño winters tend to be cooler and wetter than those in neutral years; whereas La Niña winters tend to be warmer and drier (Kiladis and Diaz, 1989; Hanson and Maul, 1991; Schmidt et al., 2001). Different ENSO phases are identified using indices of sea surface temperatures (SST) in the equatorial Pacific Ocean and associated pressure and wind pattern changes. Generally, an ENSO year is classified as El Niño if the 6 month spatially averaged mean is at least +0.5 °C greater than average, La Niña if it is −0.5 °C lower than average, and neutral otherwise, although the precise definition has changed over time and varies by study (Trenberth, 1997). In this research, categorical definitions such as the Japan Meteorological Agency's "El Niño" or "La Niña" will not be used to define entire years (JMA Atlas, 1991). Instead, the continuous SST anomaly time series averaged over the region bounded by 5°N–5°S, from 170°W to 120°W and called the NINO 3.4 index is used to encompass finer temporal variability within the ENSO signal (Trenberth, 1997). ENSO phase has previously been shown to have predictable effects on stream flow, precipitation, monsoon occurrence, crop yield, cholera occurrence, flood frequency, and simulated water quality data in different regions around the world (Chiew et al., 1998; Piechota and Dracup, 1999; Rajagopalan and Lall, 1998; Handler, 1990; Kulkarni, 2000; Hansen et al., 1997; Pascual et al., 2000; Keener et al., 2007). In monitoring and research efforts during the 20th century, ENSO indices have emerged as one of the most consistent for describing inter-annual climate variability on both global and regional scales (Ropelewski and Halpert, 1986).

Often in research, hydrological processes over long periods of time are assumed to be stationary. Observed data for many different variables provide evidence to the contrary. Spectral analysis methods have been used to investigate the frequency relationships between large scale climate indices such as the ENSO, North Atlantic Oscillation (NAO) and Pacific Decadal Oscillation (PDO) and hydrologic variables such as stream flow and precipitation (Rajagopalan and Lall, 1998; Einfield et al., 2001; D'Arrigo et al., 2001). Spectral wavelet methods allow one to explore non-stationary aspects of time series within the frequency domain.

The ENSO phenomenon is recognized as having an approximate periodicity of 3–7 years (Rasmusson and Wallace, 1983), which has various affects on global climate. If relationships shown in other locations between observed precipitation, stream flow, and the ENSO index (Rajagopalan and Lall, 1998; Labat, 2008) are valid in the Little River Watershed in Georgia, it may be possible to use the NINO 3.4 anomalies as a predictor for high risk monthly nutrient loading, and thus as part of a best management practice (BMP) or BMP selection tool. The wavelet analysis allows the characterization of the low-frequency oscillations and amplitudes associated through time with geophysical data such as rainfall, SST (Wang and Wang, 1996; Torrence and Compo, 1998), and nutrient loading. Coherence and cross-wavelet analysis then allows the direct comparison of two time series, SST and precipitation, stream flow, or nutrients, for the purpose of identifying areas in which they co-vary with high power (Grinsted et al., 2004). Investigating and identifying significant oscillation periods in precipitation, stream flow, and nutrient loads in the southeast United States that correspond to ENSO oscillations is a crucial first step in ultimately reducing risks associated with climate variability in managing water resources and agricultural systems. The result is an understanding of both recurrent, episodic phenomena, and also a method of quantitatively describing climate risk that is changing in time.

Hydrological relationships involving storm runoff and infiltration rates that apply in much of the US do not apply for the coastal plain (Sheridan et al., 2001), and it is therefore often necessary to create new models with specific hydraulic relationships for the region. Existing models often rely on empirical algorithms to represent processes that are not well understood, making wavelet analysis appealing, in which long term, high, or low frequency patterns can be found and used to advance understanding of these processes. Inclusion of the impacts of the large riparian zones in the LRW on flow and water quality is critical to accurate physical hydrological modeling (Sheridan et al., 1983). Evidence exists that seasonal precipitation in the region may be shifting, with more rainfall from September to March, and less during the growing season from April to August (Sheridan and Knisel, 1989; Baigorria et al., 2007). The southeast United States is an important region both economically, agriculturally, and socially, because of its rapidly growing population that will add water demand and environmental stress to currently stressed or degraded ecosystems. To address the multitude of issues associated with the changing climate in the southeast, finding new methods of making predictions for hydro-climatic variables based on periodic non-stationary phenomena such as the El-Niño/Southern Oscillation is an important tool. In this research, wavelet analysis explores the link between nutrient loading, hydrology, and ENSO in the Little River Watershed near Tifton, Georgia. This study is a first step in ultimately modeling how flushes of nutrient loading in the southeast may be reduced via management based on current or short-term predictions of ENSO phase.

Methods and procedures

Field site

The Little River Watershed (LRW) in Tifton, southeast Georgia, is an example of a stereotypical coastal plain watershed. Occupying a large area in the southeast US, coastal plain watersheds are characterized by broad, flat alluvial flood plains with low-gradient, poorly defined channels, sandy soils, and slow moving streams. The LRW covers 334 km^2, of which approximately 40% of the southern half and 30% of the northern half are agricultural cropland (Bosch et al., 2004). It is comprised of eight sub-basins of size varying from 9 to 115 km^2 (Fig. 1), and has extensive riparian buffers and gentle stream slopes ranging from 0.1% to 0.5%. All analyses in this paper were done on sub-basin K, a 16.8 km^2 area with 106–146 m elevation in the watershed uplands with the most comprehensive nutrient data available of the basins.

Climate in the LRW region is humid sub-tropical, characterized by long and hot summers, short and mild winters, and an average growing season of 245 days (Sheridan, 1997). Annually, the area's average precipitation (1922–1988) is 1208 ± 214 mm (Sheridan and Knisel, 1989), with variable monthly distribution. As in much of the southeast US, summer rainfall is characterized by convective storms with shorter individual events that occur with greater frequency and intensity than in other seasons. In this regard, summers in the LRW usually have total greater rainfall than other seasons (Sheridan, 1997). Typically, the fall months have the least total rainfall, but are more likely to have extended storms with longer average duration between precipitation events (Feyereisen et al., 2008). Late summer and fall months may also receive heavy rainfall from tropical storms. Winter and spring seasons receive more total rainfall than the fall season, and continue to be characterized by variable low-intensity storm events. Average tempera-

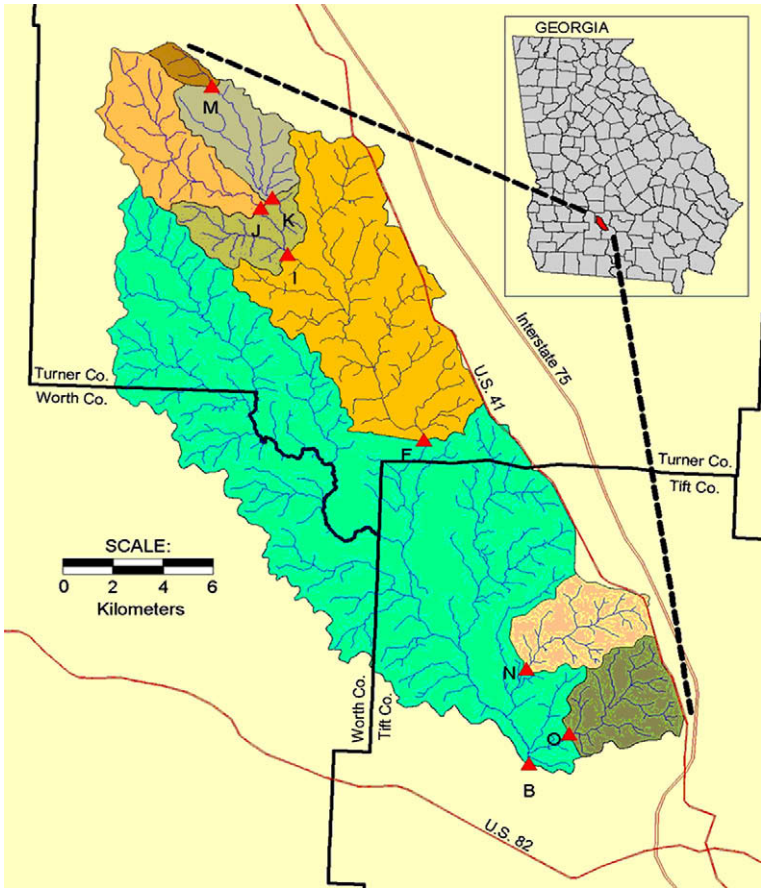

Fig. 1. The Little River Watershed and sub-basins, Tifton, Georgia. The total area is 334 km^2. All analysis was done with data from upland sub-basin K, with an area of 16.8 km^2. Triangles indicate weir/stream flow measurement locations for each sub-basin.

tures range from a monthly minimum of 4.2 °C in January to a maximum of 32.7 °C in August, with an annual average of 19.1 °C (Sheridan, 1997).

Shallow, groundwater flow is the primary runoff component in uplands, accounting for up to 80% of streamflow (Sheridan, 1997). Groundwater flow is also the primary flow route for soluble nutrients (Lowrance et al., 1984a). The soils of sub-basin K are mainly sandy loam and loamy sand with characteristically high infiltration capacity. Infiltration at the surface is restricted by a plinthic layer of clay/sandy clay loam with low hydraulic conductivity (Feyereisen et al., 2008). Groundwater recharge to aquifers below the surficial aquifer is restricted by the Hawthorn formation, which makes up the confining layer for the artesian aquifer under the watershed (Stringfield, 1966). The shallow lateral subsurface flow and groundwater flow from the surficial aquifer contribute to seasonal stream flow (Sheridan, 1997).

Sub-basin K in 1968 was defined as mixed-use agricultural, and vegetative mapping showed land use as 39% agricultural (mostly peanuts, corn, cotton, soybean, tobacco), and 61% woodland (mostly slash and longleaf pine with wiregrass or broomsedge, some hardwood pine, swamp hardwood, and pine/oak) (Sheridan et al., 1983). In 2003, the land use had changed to approximately 29% agricultural and 57% woodland (Feyereisen et al., 2007b). The Southeast Watershed Research Lab (SEWRL) in Tifton has collected hydraulic and climatic data continuously for the entire watershed since 1965, and water quality data in sub-basin K beginning in the mid-1970s (Feyereisen et al., 2008). There are also historical land-use and fertilizer records starting in the late 1970s.

Historically, the environment and water quality of the LRW has not been overly adversely affected by agricultural practices, due to the effect of large riparian filters throughout the heavily forested watershed. However, the cultivated agricultural area in sub-basin K has been increasing since the early 1990s with a related decline in upland and riparian areas, meaning that the ecology and water quality are being increasingly impacted. Because of the large amount of data available for the LRW, analysis of this impact is possible. Within the 30% of cultivated area in sub-basin K in 2004, cotton is the major crop grown, comprising 68% of all cultivated area with peanut next with only 29%. As one of the more upland sub-basins, field studies in 1984 showed that K was accumulating the most nutrients in the LRW, which suggested that more intensive cropping of the upland fields could lead to more efficient use of nutrients by having actively growing crops for more of the growing season (Lowrance et al., 1984b). Currently, almost year round production of row crops has led to extensive and sustained use of fertilizer and pesticides on the watershed (Bosch et al., 2004). On the other hand, less intensive agriculture coupled with increased forest and riparian area could have similar effects on efficient use of nutrients.

In past studies done by SEWRL, the LRW has shown the highest overall stream flow concentrations of nitrate (NO_3) and total phosphorus (P) from January to March, and minimums from July to September (Lowrance et al., 1984b). Low rainfall and low evapotranspiration, decreased denitrification and decreased uptake in the upland and riparian zones may contribute to higher nutrient concentrations in the winter, while crop nutrient uptake and low leaching may cause low concentrations in the summer (Lowrance et al., 1984a). Decreased NO_3 and P concentrations were observed during April to June even though runoff was still high and fertilizer application occurred, in part because of biological effects such as

nutrient uptake, transpiration, and utilization. Nitrate loads are highest when stream flow is highest, from December to February, and lowest when flow is least, from September to November. Nutrient loads are disproportionately low from June to August while flow is still relatively high, as crops are utilizing the most nutrients in this season (Lowrance et al., 1984b; Lowrance et al., 1985). Over the past 25 years, there have been numerous studies by SEWRL documenting the hydrology, ecology and stream chemistry of the LRW (Bosch et al., 2006; summarized in Feyereisen et al., 2008), yet nothing investigating the relationship between the hydrology and local ENSO effects.

Little River Watershed data

Observed precipitation and stream flow data from sub-basin K of the LRW used in this study ranges from February of 1968 to June of 2005, and have been recorded and compiled by researchers at SEWRL in Tifton, Georgia (Table 1). Details on the daily flow and precipitation data collection, quality, and processing are thoroughly discussed in Bosch et al., 1999, 2007; Bosch and Sheridan, 2007. Flow in the LRW is measured every 5 min at eight concrete v-notch weirs built between 1967 and 1971, one of which lies at the outlet of sub-basin K (Yates, 1976). There are currently 46 active rain gauges in the LRW, 13 of which are within and surrounding sub-basin K, and were used to calculate the weighted watershed area daily precipitation (Bosch et al., 2007). Daily precipitation data within sub-basin K were created from watershed weighted data using the methods of Dean and Snyder (1977) (Bosch et al., 2007), summed into monthly cumulative values, and then normalized by monthly average to remove annual cycles for each month of the record. Processed daily stream flow data (Bosch and Sheridan, 2007) for all 37 years were summed into monthly cumulative values and normalized by monthly average as well.

Nitrate and total phosphorous concentration datasets contain varied collection frequencies from 1974 to the present, ranging from every 5 min to once a week. Researchers at SEWRL have infilled the nutrient data to the daily level using a variety of methods based on the sampling method that was used (i.e. automatic sample, manual grab). The in-filling provided complete daily time series of 24 years of total P concentration (from January, 1979 to December, 2003), and 29 years of NO_3 concentration (from January, 1974 to December, 2003). The detailed methods and reasoning behind stream chemistry in-filling are discussed in Feyereisen et al., 2007a, and additionally located on the LRW public database website, located at ftp://www.tiftonars.org/, under the file "streamchemistry_readme.txt". Daily concentration data were converted to loads by multiplying daily flow by nutrient concentration. Nutrient concentrations and loads were average into basin-wide monthly values and normalized by median monthly values, creating time series of averaged monthly anomalies with the annual cycle removed. Median values were used to normalize nutrient concentrations and loads to minimize difficulties associated with the different methods of nutrient data in-filling.

Sea surface temperature anomalies were calculated from the Kaplan extended NINO 3.4 index (27.5–22.5°E and 87.5°S–87.5°N), which is available from the Lamont–Doherty Earth Observatory data library (Table 1) (Kaplan et al., 1998). The SST data are gridded by $5° \times 5°$ delineations, and range from 1856 to the present, although only the 1968–2005 data are used in this study. Temperatures were converted to monthly average and seasonal average anomalies by being normalized against the total month's average. All variables' raw time series were plotted against time (month and year) to provide an initial visualization of the data trends (Fig. 2).

Wavelet analysis

Wavelet analysis is a spectral method of decomposing a time series into time and frequency space, allowing the identification and analysis of dominant localized variations of power, i.e., where the variance of the time series is largest for a given frequency. In this context, a main purpose of using the wavelet analysis technique is to quantify and visualize statistically significant changes in the ENSO SST and nitrate load variance over a multi-decadal time scale. The windowed Fourier transform is typically used to analyze a signal in frequency space at a global level, however, it is scale-dependant, and is hence inefficient and inaccurate when attempting to perform an analysis on non-stationary environmental data sets with different signal powers that evolve through time (Torrence and Compo (1998)). A well known and relevant example is that of SST's in the equatorial Pacific Ocean, where the dominant mode of variability is ENSO, shown by frequency signals on a time scale of 3–7 years (Rasmusson and Wallace, 1983). Superimposed on this signal are much longer inter-decadal fluctuations, visible in the wavelet power spectrum over time as the evolution of the SST signal power. The inter-decadal fluctuations have the effect of modulating the amplitude and frequency of occurrence of El Niño events. Torrence and Compo (1998) have written a comprehensive guide to wavelet use for geophysical data, the basic theory they discuss will be summarized here.

With any time series, $x_n (n = 0, \ldots, N-1)$ with time spacing δt, there is a corresponding wavelet function, $\psi_o(\eta)$, with zero mean and localized in time and frequency space, that depends on a non-dimensional time parameter, η, and the non-dimensional frequency, ω_0. In this analysis, the Morlet wavelet (Eq. (1)), consisting of a plane wave modulated by a Gaussian, is used for all time series, the frequency of which, in practice, is given the default value of $\omega_0 = 6$ for all analyses (Farge, 1992):

Table 1
LRW time series data and sources used.

Variable	Years	Source	Comments
NINO 3.4 SST (°C)	1968–2005	Kaplan extended index, http://ingrid.ldeo.columbia.edu/SOURCES/.KAPLAN/.EXTENDED/.ssta/	Anomaly data averaged monthly
Precipitation (mm)	1968–2005	ftp://www.tiftonars.org/databases/LREW/Precipitation/Daily	Summed, averaged and normalized monthly. Some in-filled values
Stream flow (m^3)	1968–2005	ftp://www.tiftonars.org/databases/LREW/streamflow/daily	Daily values averaged and normalized monthly. Some in-filled values
NO_3 concentration (mg/L)	1974–2003	ftp://www.tiftonars.org/databases/LREW/stream_water_quality/long_term_water_quality	Daily/weekly values averaged and normalized by median monthly. Some In-filled data
NO_3 load (kg)	1974–2003	ftp://www.tiftonars.org/databases/LREW/stream_water_quality/long_term_water_quality	Daily/weekly values averaged and normalized by median monthly

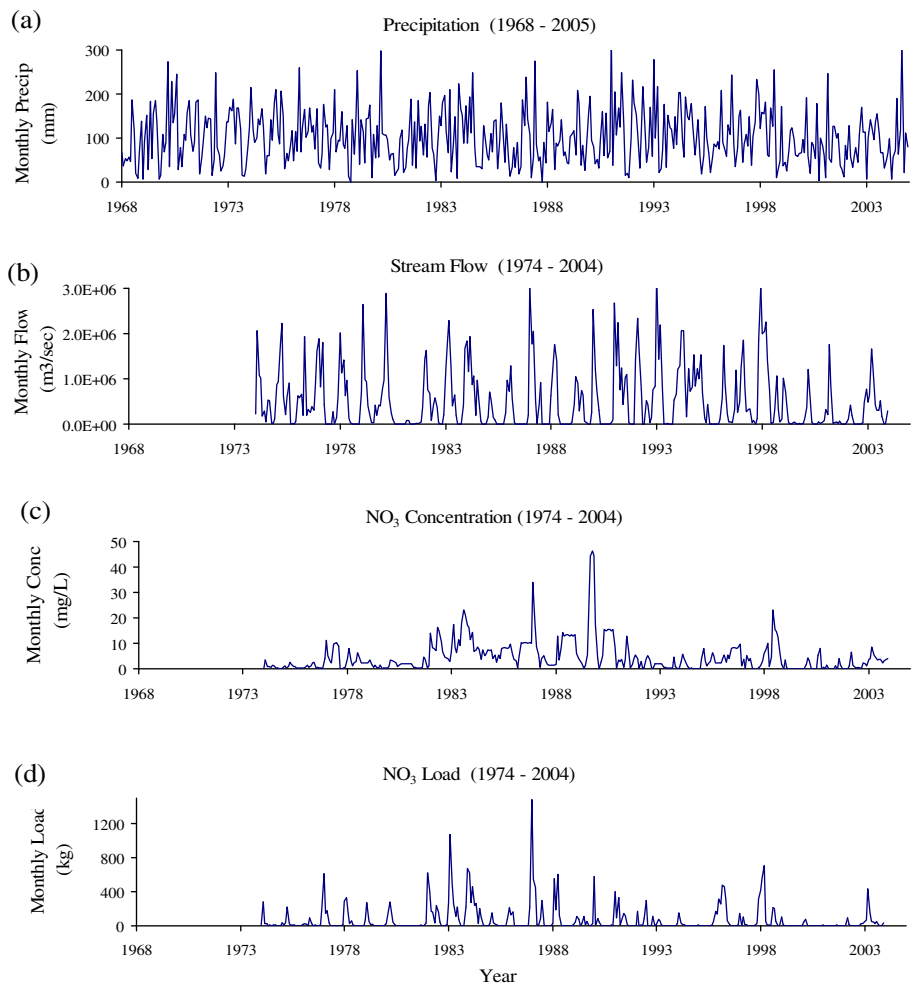

Fig. 2. Raw monthly time series of (a) precipitation (mm), (b) stream flow (m^3/s), (c) NO_3 concentration (mg/L) and (d) NO_3 load (kg).

$$\Psi_0(\eta) = \pi^{-1/4}\exp^{i\omega_0\eta}\exp^{-\eta/2} \tag{1}$$

A Morlet wavelet is a non-orthogonal, complex function that can be used with the continuous wavelet transform, $W_n(s)$. The continuous wavelet transform (Eq. (2)) of a discrete sequence x_n, is the convolution of x_n with a scaled and translated version of $\psi_o(\eta)$:

$$W_n(s) = \sum_{n'=0}^{N-1} x_{n'}\psi^*[(n'-n)\delta t/s] \tag{2}$$

where $(*)$ is the complex conjugate, s is the wavelet scale, n is the localized time index, n' is the translated time index, and ψ is the normalized wavelet. An approximate value of W_n can be found by performing the convolution N times for each scale, where N is the number of points in the time series. All convolutions can then be done in Fourier space using a discrete Fourier transform of x_n, (Eq. (3)), which in our case, is:

$$\hat{x}_k = (1/N)\sum_{n=0}^{N-1} x_n \exp^{-2\pi ikn/N} \tag{3}$$

where $k = (0, \ldots, N-1)$ is the frequency index. By the convolution theorem, the wavelet transform (Eq. (4)) is the inverse Fourier transform of the product of the discrete Fourier transform of x_n and Ψ^*, with angular frequency ω_k:

$$W_n(s) = \sum_{k=0}^{N-1} \hat{x}_k\hat{\psi}^*(s\omega_k)\exp^{i\omega_k n\delta t} \tag{4}$$

Finally, the wavelet power spectrum is defined as $|W_n(s)|^2$, and the amplitude at each point, $|W_n(s)|$ and phase, $\tan^{-1}[I\{W_n(s)\}/R\{W_n(s)\}]$ can be found. Significance levels for wavelet spectra are found by comparison against a random background distribution, which, for geophysical spectra, are modeled as either white or red noise (increasing power with decreasing frequency). In this study, red noise is used (Wang, 1995; Torrence and Compo, 1998), and modeled as a univariate lag-1 autoregressive (AR-1) process.

The wavelet variance is indicated by the Global Wavelet Spectrum (GWS), calculated by the integration of the squared transform coefficients at different scales for all data points. Areas of global wavelet significance are shown as a dashed blue line, above which indicates a 95% confidence limit above red noise. Continuous Morlet wavelet transforms and wavelet power spectra were computed and visualized for all monthly normalized time series in Table 1 to find significant periodicities that correspond to ENSO signals. All univariate wavelet analysis was done using the WAVETEST Matlab script for WAVELET (Torrence and Compo, 1998), which can be downloaded from: http://paos.colorado.edu/research/wavelets/.

Cross-wavelet and coherence transforms

A detailed explanation of cross-wavelet transform (XWT) can be found in Torrence and Compo (1998). Given two different time series, X and Y, with different wavelet transforms $W_n^X(s)$ and $W_n^Y(s)$, the cross-wavelet transform is $W_n^{XY}(s) = W_n^X(s)\ W_n^{Y*}(s)$, where $(*)$ denotes the complex conjugate. The spectrum is complex, thus

the cross-wavelet power can be defined as $|W_n^{XY}(s)|$. The cross-wavelet transform finds regions in time frequency space where the two time series show high common power, and thus, significance. In particular, this transform examines whether regions in time frequency space with large common power have a consistent phase relationship, and therefore are suggestive of causality between the time series (Grinsted et al., 2004).

Computing the wavelet-coherence transform (WTC) finds regions in time frequency space where the two time series co-vary, but do not necessarily have high power. For this reason, both the cross-wavelet transform and the wavelet-coherence transform are necessary when analyzing two time series to assess both causality and local co-variance. Generally, a WTC will have more significant areas than an XWT figure, as the significance is sacrificed for the desirable visualization of shared power in the XWT. From Torrence and Compo (1998), the wavelet-coherence transform of two time series (Grinsted et al., 2004) is defined as:

$$R_n^2(s) = \frac{|S(s^{-1}W_n^{XY}(s))|^2}{S(s^{-1}|S(W_n^X(s))|^2) \cdot S\left(s^{-1}|S(W_n^Y(s))|^2\right)} \tag{5}$$

where S is a smoothing operator defined by the wavelet type used and the entire expression is similar to that of a traditional correlation coefficient localized in time–frequency space. The statistical significance level of the wavelet coherence is estimated using Monte Carlo methods, and then the significance level for each scale is calculated using only values outside the cone-of-influence.

Cross-wavelet and coherence transforms were done on normalized NINO 3.4 SST time series with precipitation, stream flow, NO_3 concentration and NO_3 load, all calculated to 95% significance levels. Wavelet coherence and cross-wavelet software used was via the XWT and WTC scripts written by Aslak Grinsted for Matlab, © 2002–2004, downloadable at http://www.pol.ac.uk/home/research/waveletcoherence/.

Cross-correlation time series analysis

The lagged cross-correlation between the ENSO index and the hydrological time series, $x(i)$ and $y(i)$, at different delays ($d = 0, \ldots, N-1$) were computed as:

$$R = \frac{\sum_i \left[(x(i) - \mu_x) * (y(i-d) - \mu_y)\right]}{\sqrt{\sum_i (y(i-d) - \mu_y)^2}\sqrt{\sum_i (x(i) - \mu_x^2)}} \tag{6}$$

In which N is the length of the time series and μ_x and μ_y are the respective means. A positive correlation is associated with the series correlated in their current configuration, while a negative correlation indicates a relationship with the inverse of one of the time series. The delay at which maximum correlation is seen describes the most significant time lag relationship between the two data series. Cross correlations were calculated between the NINO 3.4 SST time series and precipitation, stream flow, NO_3 concentration and NO_3 load for delays from 0 to 24 months. Significance was calculated at 95% confidence corrected for time series autocorrelation (World Meterorological Organization, 1966).

Results

Wavelet analysis

The monthly wavelet power spectra for the NINO 3.4 SST, precipitation, stream flow, and NO_3 concentration and load time series are shown in Fig. 3a–e. As previously demonstrated (Wang and Wang, 1996; Torrence and Compo, 1998), when the annual cycle is removed, SST power (Fig. 3a) is concentrated within the ENSO periodicity band of 3–7 years, although the amplitude and dominant modes tend to shift through time. From 1911 to 1960, a 5–7 year period is strongest, while a 4–5 year period dominates from 1972 to 1992 (Wang and Wang, 1996). Longer decadal variations cannot be assessed with significance given the limited length of record. The annual cycle of ENSO is associated with observing strong La Niña power in the wavelet spectrum (Wang and Wang, 1996), as well as normal seasonal variations (Baldwin et al., 2001). The enhancement of annual power by La Niña, and respective weakening during El Niño, has been hypothesized to be due to the thermocline becoming shallower and the trade winds strengthening, which reinforces the ocean upwelling effect that modulates the annual SST cycle (Gu and Philander, 1995). Therefore, by removing the annual cycle, we are able to more easily visualize powerful El Niño events in the 3–7 year band. The most pronounced SST variability within the wavelet power spectrum is observed during the strongest El Niño phenomena encompassed within this time series, namely the 1982–1983 and 1997–1998 events—the latter of which is the strongest El Niño recorded in the 20th century (Chavez et al., 1999).

Precipitation in the southeast US and the LRW has distinct seasonality. In the coastal plain region and more specifically the LRW, the most intense precipitation events are in the spring and summer months, associated with convective or cyclonic storms (Sheridan, 1997). Summer events are shorter, smaller in area, and more frequent and intense, while fall and winter events are frontal in nature, milder, but longer in duration. The wavelet power spectrum of monthly precipitation anomalies from 1968 to 2004 is shown in Fig. 3b. Low frequency precipitation information corresponding to the 3–7 year ENSO signal has been demonstrated in the Florida Everglades via wavelet analysis, as well as in the western US, (Kwon et al., 2006; Rajagopalan and Lall, 1998), and the Little River Watershed shares that signal. Regions of high power relative to the noise background are seen in the precipitation record in the same 3–7 year periodicity as for the NINO 3.4 series (Fig. 3b), although the signal is not powerful enough for statistical significance, nor is it as clear as the SST record in Fig. 3a. Since a 4–5 year quasi-periodicity dominates ENSO from 1972 to 1992 as seen in longer SST wavelet analyses (B. Wang, 1995; Wang and Wang, 1996), this may explain the 4–5 year period visible in the precipitation time series. Again, the strongest power at that frequency is seen from 1981 to 1992 and surrounding the 1997–1998 El Niño event, which implies that ENSO variability clearly is associated with precipitation in basin K of the LRW (Fig. 3b). The high power still visible at the 1–2 year period, despite removal of the annual cycle, may represent the variability from a seasonal anomaly. Analyzing summer and winter seasons separately with each hydrological variable showed slightly stronger 3–7 year ENSO wavelet power in winter months, although not enough to be statistically significant.

In basin K of the LRW, average annual stream flow depth is approximately one-third of annual precipitation (Sheridan, 1997; Feyereisen et al., 2008), a figure comparable to similar statistics from other coastal plain watersheds. As such, the inter-annual component of the wavelet power spectrum (Fig. 3c) for the stream flow record for 1974–2003 shares much of the power and variability pattern seen in the precipitation spectrum, although the signal is actually stronger as it is less noisy than the precipitation record. The ENSO periodicity is seen again as high power in stream flow for the 3–7 year period, surrounding the 1982–1983 and 1997–1998 El Niño events. High power is again seen in the 1–2 year period, perhaps related to intense summer storms. Clearly, the observed 3–7 year periodicity in the stream flow spectrum demonstrates that while ENSO signals have been found in large rivers around the world (Chiew et al., 1998; Labat, 2008), the relationship is valid for small, slow-moving coastal plain streams and rivers in the LRW as well.

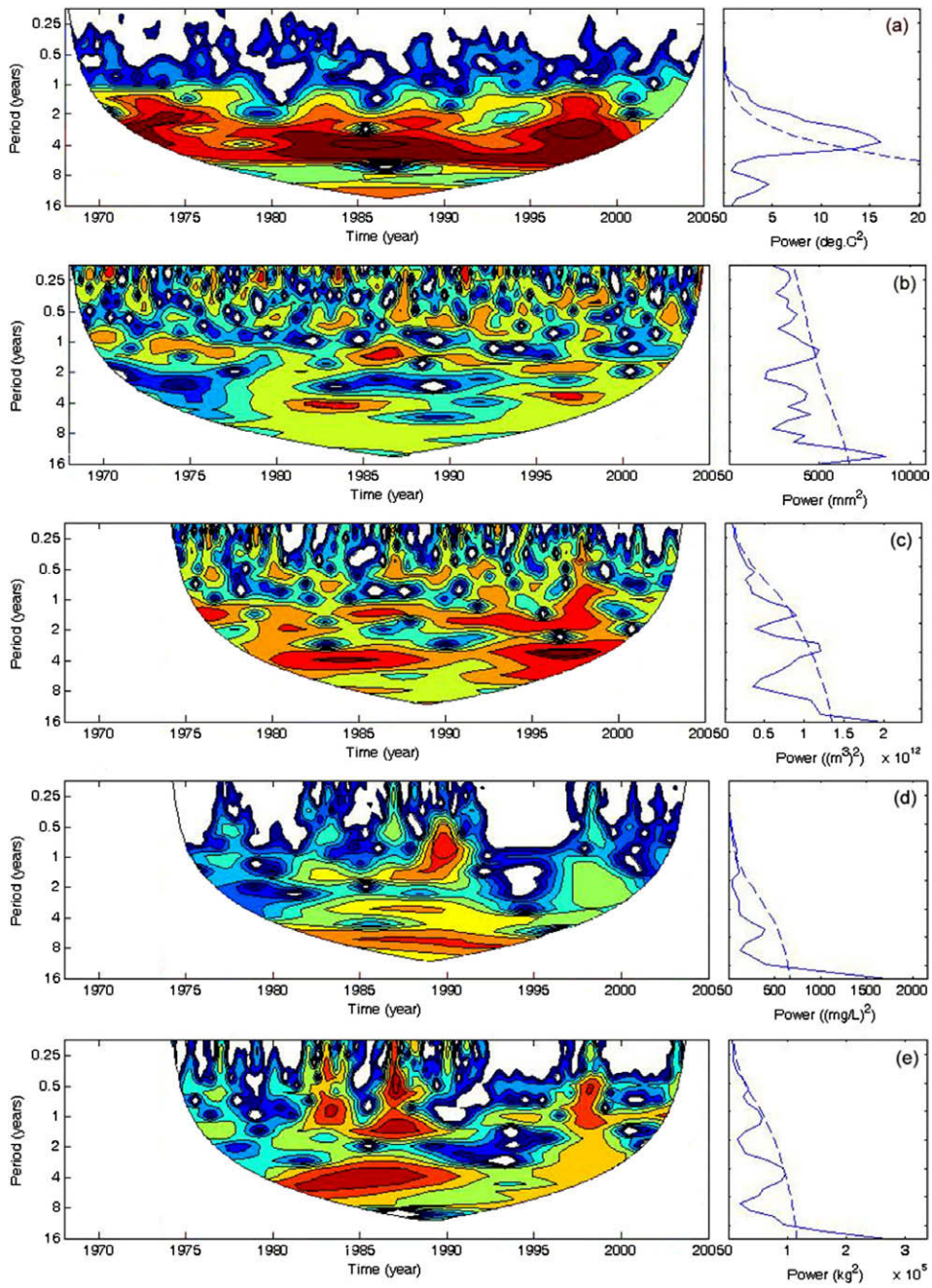

Fig. 3. Significant Wavelet Power Spectra are shown within the cone-of-influence, which depends on time series length and degrees of freedom. Figures are color-mapped to indicate high wavelet power with reds and oranges, and low powers in blue and white. The Global Wavelet Spectrum (GWS) at the right of each figure shows power integrated over all scales and times. The 95% confidence limit is shown on the GWS (dashed blue line), the periodicities above which show significance. (a) Monthly NINO 3.4 (°C) sea surface temperatures, (b) monthly precipitation anomaly (mm), (c) monthly stream flow anomaly (m^3), (d) monthly NO_3 concentration anomaly (mg/L), and (e) monthly NO_3 load anomaly (kg).

Wavelet power spectra of nitrate concentration (mg/L) and load (kg) are shown in Fig. 3d and e, respectively. While it has been shown that categorical ENSO signals exist in model simulated nutrient loads in south Florida (Keener et al., 2007), observed and continuous data have not been analyzed in the literature. Both nutrient series extend from 1974 to 2003. NO_3 concentration exhibits less marked high power in the ENSO periodicity than either precipitation or stream flow, which is expected due to a less direct relationship with the atmosphere. There is also high power centered on the 1988–1989 La Niña, at 1–2 year periodicity, and may signify an anomalous event. These regions of high variability imply that NO_3 concentration is more sensitive to the high intensity rains characteristic of La Niña summers or hurricane in the southeast, although no periods are significant at the 90% level as manifested in the global wavelet spectra. The minimal concentration power visible indicates that the concentration signal does not change in a significant or systematic way, and that flow and load should remain the main focus.

Nitrate load (Fig. 3e) is a combination of stream flow and concentration spectra. Accordingly, there is a broader band of ENSO-related high power in the 3–7 year period centered on the 1982–1983 El Niño, and only medium power visible in the cone-of-influence around the 1997–1998 El Niño. A longer time series may reveal more about the load structure during the latter El

Niño. High power is seen in nitrate load in the 1–2 year periodicity centered around 1986–1989, which may reflect the stream flow's modulation of the concentration, and the La Niña event of 1998–1999, the pattern of which is also reflected in high power seen in precipitation, stream flow, and SST spectra. This may again be related to the high annual power noted in some strong La Niña or seasonal events (Wang and Wang, 1996).

Cross-wavelet analysis

Although one can see regions in the wavelet power spectra in the previous section where two time series show high common power, a more direct analysis of two series is needed. Significance levels of the cross-spectra power are calculated against a red noise background, indicated by thick black outlines in the cross-wavelet transform figures (Fig. 4a–d) to the 5% level. The cross-wavelet transform between SST and precipitation (Fig. 4a) shows that areas that were picked out as possibly sharing power in the single wavelet spectra, do indeed share significant power in the 3–7 year periodicity surrounding the 1982–1983 and 1997–1998 El Niño. The significant areas within the 3–7 year period are phase-locked positively, which when considered with the fact that ENSO is a main driver of global climate variation, suggests a causal relationship between SST and precipitation in the LRW that was already suspected. The same patterns of shared power, phase, and 3–7 year periodicity are seen in the cross-wavelet transform between SST and stream flow (Fig. 4b).

The cross-wavelet transform relationship between NO_3 concentration and SST (Fig. 4c) shows less significant shared power, although there is a small area from 1985–1990 around 3–4 year periodicity. The general 3–7 year period area shows high power, but too little for significance at the 5% level. The lack of definitive relationship between SST and concentration is explained by nutrient concentrations being very much an extraneous variable, dependent on both local agricultural activities and rainfall or river flow. Nutrient load, on the other hand, takes stream flow into account. The cross-wavelet transform of NO_3 load and SST (Fig. 4d) shows the same significant area as the cross-wavelet transform with stream flow and precipitation, a shared 3–7 year in-phase periodicity extending from 1980 to 1990, and a 1–2 year periodicity in the area around the 1998–1999 La Niña.

Wavelet coherence analysis

Compared with the cross-wavelet transform, a larger area in the wavelet coherence figures is marked as significant. However, neither the significance of the wavelet-coherence transform nor the cross-wavelet transform on their own do not necessarily imply causality, as any two variables can be significantly correlated by chance. Small areas of wavelet-coherence transform significance are unlikely to be causal taken on their own. More extensive areas of significance, however, are less likely to be due to chance, and should be examined carefully for additional relationships to a physical mechanism. The wavelet-coherence transform between SST and precipitation (Fig. 5a) and SST and stream flow (Fig. 5b) show very similar sustained significant areas from 1979–2000 in the 3–7 year period, indicating high correlation between SST and each time series in the area relating to ENSO signal. Longer time series would be desirable for every variable to further investigate the changing periodicities; however within the cone-of-influence, there is a sustained ENSO signal.

The wavelet-coherence transforms between NO_3 concentration and SST is shown in Fig. 5c. There are arguably no areas of causal significance, especially when considered with respect to the importance of variables outside of this analysis such as fertilizer application or land-use changes. Practically, this means that the two time series do not show any significant correlation at any periodicities of interest to this study, although there is a

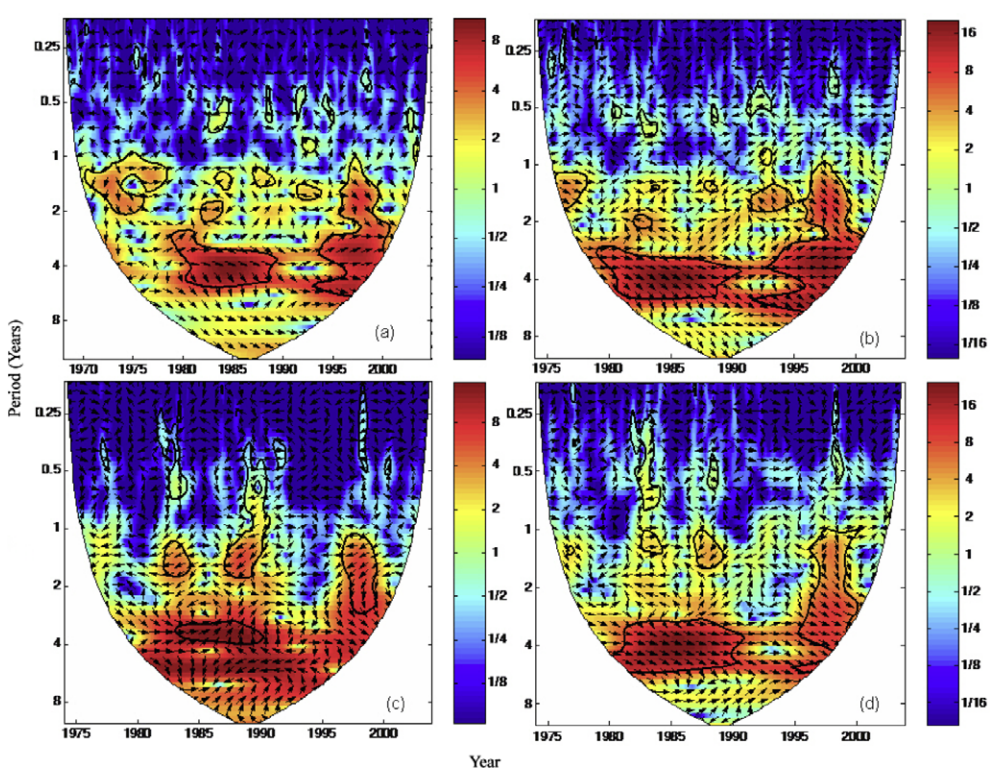

Fig. 4. Cross Wavelet Spectrum between (a) monthly SST and Precipitation, (b) monthly SST and stream flow (m^3), (c) monthly SST and NO_3 concentration (mg/L), and (d) monthly SST and NO_3 Load (kg). Black figure outlines indicate areas significant to 95% confidence, while arrows represent variables' phase relationship. Arrows pointing clockwise indicate in-phase behavior, while counter clockwise arrows indicate anti-phase behavior.

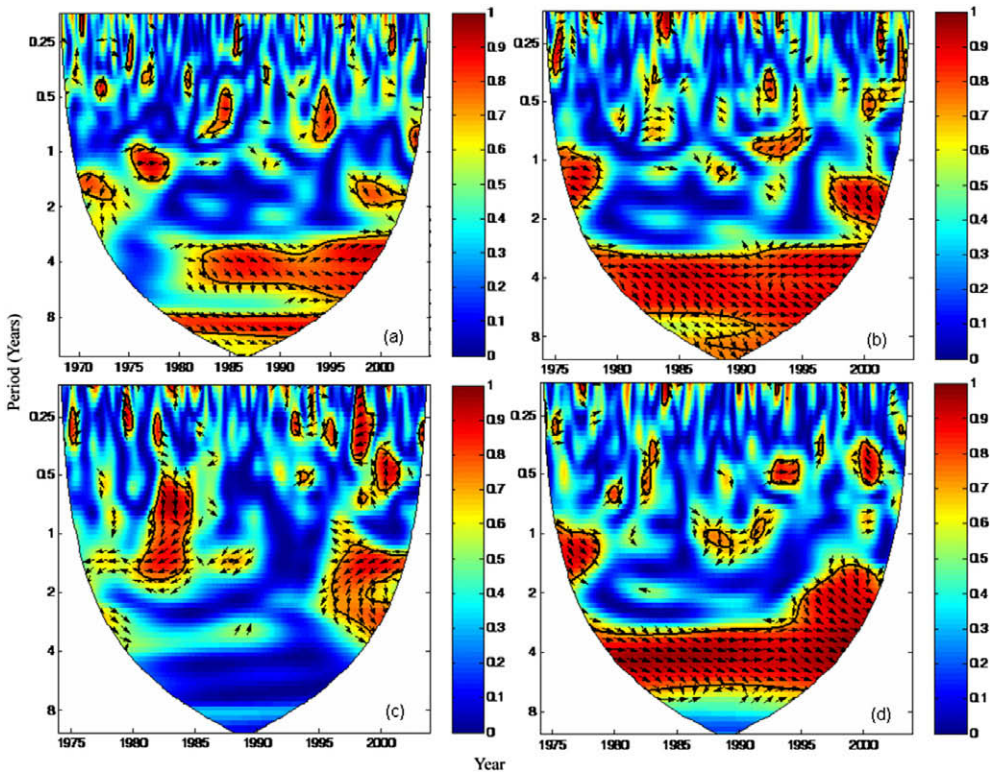

Fig. 5. Wavelet Coherence Analysis between (a) monthly SST and Precipitation, (b) monthly SST and stream flow (m^3), (c) monthly SST and NO_3 concentration (mg/L), and (d) monthly SST and NO_3 load (kg). Black figure outlines indicate areas significant to 95% confidence, while arrows represent variables' phase relationship. Arrows pointing clockwise indicate in-phase behavior, while counter clockwise arrows indicate anti-phase behavior.

small area of ENSO related significance in the XWT. The concentration significance in the XWT may be a remaining artifact from the much stronger stream flow signal seen in Figs. 4 and 5b, showing up despite the stochastic nature of the concentration series. When analyzed in conjunction with the WTC, it becomes clear that this is probably an artifact and should not be assigned any causal explanation. Nitrate load, however, (Fig. 5d) shows a very high correlation with SST throughout all the years within the cone-of-influence at 3–7 year periodicity. This correlation reflects a combination of the strong stream flow ENSO signal with the weak concentration ENSO signal, but should not be discounted as non-causal, as stream flow response is directly related to precipitation and SST. The in-phase correlation and power of SST and NO_3 load suggests that a model based upon the 3–7 year periodicity of ENSO could have predictive skill for LRW nitrate loads. Across all the wavelet power analyses, the ENSO signal appears in sustained and common 3–7 year frequency bands. This frequency structure is replicated across the NINO 3.4, precipitation, stream flow, and NO_3 load time series, and is moreover found within the cross-wavelet and wavelet

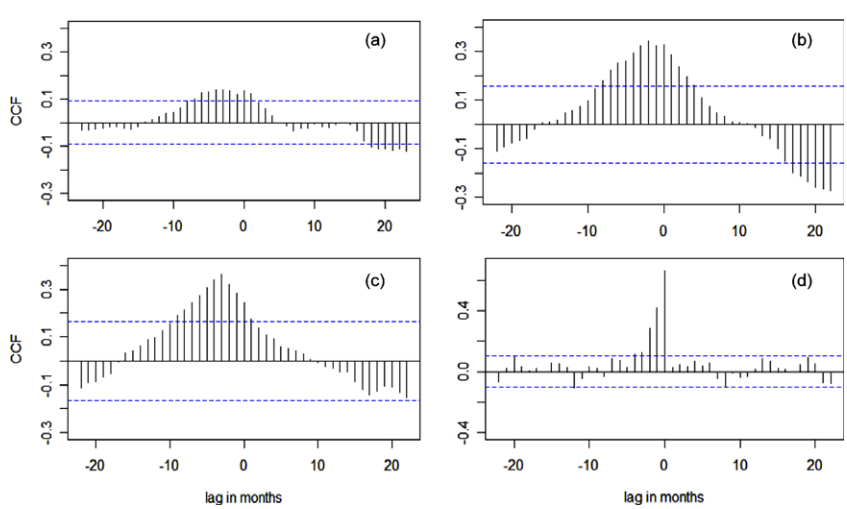

Fig. 6. Cross-correlation analysis between NINO 3.4 (°C) and LRW sub-basin K (a) precipitation (mm) (b) stream flow (m^3) (c) NO_3 (kg), and between (d) precipitation (mm) and stream flow (m^3). A negative lag indicates months that the NINO 3.4 SST leads the variable in question. The strongest cross-correlation function (CCF) relationship within the NINO 3.4 index is SST leading stream flow by two months, while the strongest hydrologic relationship overall is between precipitation and stream flow. Values above or below dashed lines indicate significant correlation above 95% confidence, corrected for autocorrelation.

coherence spectra, supporting this ENSO structure and demonstrating that the ENSO climate teleconnection extends to precipitation, hydrology, and observed NO_3 loads in the small streams of the LRW.

Cross-correlation analysis

As common frequency bands and high or significant power were found in wavelet analysis of SST and precipitation, stream flow, and NO_3 load, time series cross-correlation analysis was performed to temporally quantify how these relationships actually manifest during the year. After the removal of annual trends from each variable considered, significant monthly correlations were found between SST and all hydrological variables (Fig. 6a–c) The correlation of highest magnitude is between SST and NO_3 load (Fig. 6c), which is reinforced by the wavelet-coherence transform analysis in Section "Wavelet coherence analysis". All cross-correlations were dominated by significant positive correlations with the ENSO 3.4 index. Precipitation and stream flow had maximum cross-correlation function (CCF) values of 0.139 and 0.342 with SST at a four month and two month lag, respectively, and NO_3 load a maximum of 0.360 at a three-month lag. This means that high or low precipitation and stream flow are correlated with high or low sea surface temperature observed four and two months earlier, while NO_3 load is positively correlated with SST three months prior—observations that are supported by the cross-wavelet transform and wavelet-coherence transform spectral analyses.

Additional cross-correlation analyses were done to determine the strength of the lag relationship between precipitation and stream flow, precipitation and NO_3 load, and stream flow and NO_3 load. In each relationship, the most significant lag was at zero months, suggesting that a smaller time-step may be needed to assess the correlative lag more accurately. However, the strongest CCF value of 0.663 (Fig. 6d) was seen between precipitation and flow at lag zero, followed by stream flow and NO_3 load with a CCF of 0.472, and finally precipitation and load with 0.268. These values show that the NO_3 load is most directly correlated with flow, which supports the previous wavelet analyses.

Summary and conclusions

This paper uses wavelet analysis to identify and quantify the significance of a teleconnection between sea surface temperatures associated with the NINO 3.4 index and precipitation, stream flow, and nitrate concentration and load in the Little River Watershed in Georgia. We found common areas of high power and time series inter-annual variability manifested in the ENSO signal for 36 years of LRW monthly precipitation data, and 29 years of stream flow, nitrate concentration and nitrate load data. Areas of the highest power for all hydrological variables were observed in the 3–7 year periodicity known to be related to ENSO modes of variability. Temporally, the area of greatest variability was centered on the 1997–1998 El Niño event, which is on record as the strongest anomaly in the 20th century. Sea surface temperatures dramatically decreased from the transition of the 1997–1998 El Niño to the 1998–1999 La Niña, which may be reflected in the anomalous variability visible in the wavelet power spectra of the hydrologic variables. Nitrate concentration was the variable with the weakest ENSO signal power, which is due to it being more dependent on extraneous variables such as human-caused agricultural activities. High or significant power was seen in precipitation, stream flow, and nutrient loads in the 1–2 year period centered on the 1998–1999 La Niña, and may be related to strong seasonal signals. The stronger power seen in nitrate load time series, rather than concentration or precipitation, suggest that stream flow variability dominates the trends seen in loads.

Regions of shared power were found between the NINO 3.4 index and the hydrological variables of interest. There was common high power and phase in the 3–7 year mode of variability for strong El Niño events, as well as in the 1–2 year mode of variability for strong La Niña episodes for SST and precipitation, stream flow, and nitrate load. High time series co-variance exists in the same 3–7 year period for SST and precipitation, stream flow, and nitrate loads. The cross-wavelet transform and wavelet-coherence transform confirm that the known physical mechanism of ENSO teleconnection in the southeast United States (Schmidt et al., 2001; Ropelewski and Halpert, 1986) is causally linked to inter-annual variability within precipitation, stream flow, and nitrate load signals in the LRW. The high shared power and significant correlation between these variables confirms that the ENSO teleconnection seen in the precipitation and stream flow signals in large river and watershed systems around the world (Chiew et al., 1998; Rajagopalan and Lall, 1998; Handler, 1990; Kulkarni, 2000; Hansen et al., 1997; Pascual et al., 2000) extends to the hydrology and, more interestingly, nitrate loads in a small basin of the Little River Watershed.

Mechanistically, El Niño (La Niña) events result in increased (decreased) sea surface evaporation. The mid-latitude jet is displaced equatorially (poleward), increasing (decreasing) winter frontal precipitation in the southeast United States. Additional winter moisture is advected into the southeast from the tropical Pacific by the sub-tropical jet stream (Ropelewski and Halpert, 1986). Precipitation in El Niño winters typically increase as a result, and as seen in the large El Niño events centered around 1985 and 1997–1998 in the LRW, resulted in increased river discharge and pollution transport. It is unusual that the ENSO signal is more visible in the stream flow and nitrate loads of the LRW than in the precipitation signal. Although the thirteen weather stations used to form the precipitation series in this research are well distributed across the 16.8 km^2 area of basin K in the LRW, spatial variability of rainfall in the southeast United States is great, and still does not encompass all of the variability inherent in the watershed. For this reason, the ENSO signal present in the precipitation record may be somewhat damped, especially when considered next to the stream flow record. In addition to being a smoothed function of precipitation, stream flow in the Little River Watershed may be amplifying the ENSO signal. As has been previously discussed, groundwater flow in the LRW is responsible for up to 80% of the total stream flow (Sheridan, 1997), as well as comprising the main route for movement of soluble nutrients (Lowrance et al., 1984b). The ENSO signal in stream flow may be amplified by the significance of the role of groundwater, and additionally amplified due to the presence of the Hawthorn confining layer, restricting flow into the aquifer system and increasing the amount of lateral groundwater flow represented in the stream flow record.

The nature of the strong ENSO power visible in the wavelet analyses demonstrates that in the LRW during anomalous ENSO phases, BMP's and crop management practices could be more effectively applied to reduce the risk of high nutrient runoff resulting from the increased precipitation and stream flow. Best Management Practices in the LRW have mainly been comprised of crop rotations designed to more effectively use available water and prevent nutrient leaching. At this point, conservation tillage or crop cover practices have not been implemented in sub-basin K. Some BMP modeling work with SWAT has been done in sub-basin K, in which a simulated increase of 30% cultivated area with better crop management showed a 17% reduction in total nitrogen load (Cho et al., submitted for publication), suggesting that BMP's could in fact be quite effective in generally reducing loads.

While sometimes it is both economically as well as environmentally in a farmer's best interest to implement BMP's, it can be difficult to quantify the effectiveness of the results and for farmers to know when best to apply them. The strong ENSO signal in the nitrate load and stream flow, coupled with the cross-correlation analysis (Section "Cross-correlation analysis") of SST's suggests that when an anomalous ENSO phase is predicted or is occurring, BMP's could be put in place to control the risk of high nutrient runoff. The ability to make management decisions months in advance with reduced uncertainty of the BMP's not being needed could save the farmer both time and money, and result in environmental and water quality improvements. Implementing and monitoring the effectiveness of different BMP's in the LRW in different seasons and ENSO phases would take additional time and effort, but would be worth verifying if BMP application by ENSO phases would actually save time and money for watershed managers, farmers, or other stakeholders.

In this study, more than 29–36 years of data would have been informative as to how inter-decadal variability affects hydro-climatic events. However, short-term inter-annual climate variability is a crucial factor affecting climate in the southeast US, and therefore must be understood in how it ultimately relates to water quality. Additional large El Niño and La Niña anomalies within the hydrological time series record will also help to confirm patterns in the time and frequency domain. As a correlation has been established linking ENSO to precipitation, stream flow, and nutrient load in the LRW, a predictive model for nitrate load based on the NINO 3.4 sea surface temperatures could be utilized. By analogy, time series of different pollutant loads affecting water quality could be analyzed using these methods. Generating a forecast system for nutrient loads or other pollutants based on ENSO phenomena will be useful, feasible, and could avoid uncertainty associated with possible misrepresentation of physical processes and used in conjunction with hydrological models for the southeast coastal plain.

Acknowledgements

The research was supported in part through grants from the National Oceanic and Atmospheric Administration – NOAA – Climate Program Office (NOAA-CPO) Grant Number NJ17RJ1226, the US Department of Agriculture – Cooperative State Research, Education, and Extension Services (USDA-CSREES) Grant Number 2009-38890-19911, and developed under the auspices of the Southeast Climate Consortium (SECC).

References

Baigorria, G.A., Jones, J.W., O'Brien, J.J., 2007. Understanding rainfall spatial variability in the southeast USA. International Journal of Climatology 27 (6), 749–760. doi:10.1002/joc.1435.

Baldwin, M.P., Gray, L.J., Dunkerton, T.J., Hamilton, K., Haynes, P.H., Randel, W.J., Holton, J.R., Alexander, M.J., Hirtota, I., Horinouchi, T., Jones, D.B.A., Kinnersley, J.S., Marquardt, C., Sato, K., Takahashi, M., 2001. The quasi-biennial oscillation. Reviews of Geophysics 39 (2), 179–229.

Bates, B.C., Kundzewicz, Z.W., Wu, S., Palutikof, J.P. (Eds.), 2008. Climate Change and Water. Technical Paper of the Intergovernmental Panel on Climate Change, IPCC Secretariat, Geneva, 210 pp.

Bosch, D.D., Sheridan, J.M., 2007. Stream discharge database, Little River Experimental Watershed, Georgia, United States. Water Resources Research 43, W09473. doi:10.1029/2006WR005833.

Bosch, D.D., Sheridan, J.M., Batten, H.L., Arnold, J.G., 2004. Evaluation of the SWAT model on a coastal plain agricultural watershed. Transactions of the ASABE 47 (5), 1493–1506.

Bosch, D.D., Sheridan, J.M., Davis, F.M., 1999. Rainfall characteristics and spatial correlation for the Georgia Coastal Plain. Transactions of the American Society of Agricultural Engineering 42 (6), 1637–1644.

Bosch, D.D., Sheridan, J.M., Marshall, L.K., 2007. Precipitation, soil moisture, and climate database, Little River Experimental Watershed, Georgia, United States. Water Resources Research 43, W09472. doi:10.1029/2006WR005834.

Bosch, D.D., Sullivan, D.G., Sheridan, J.M., 2006. Hydrologic impacts of land-use changes in Coastal Plain watersheds. Transactions of the ASABE 49 (2), 423–432.

Chavez, F.P., Strutton, P.G., Friedrich, G.E., Feely, R.A., Feldman, G.C., Foley, D.G., McPhaden, M.J., 1999. Biological and chemical response of the equatorial Pacific Ocean to the 1997–98 El Niño. Science 286 (5447), 2126–2131.

Chiew, F.H.S., Piechota, T.C., Dracup, J.A., McMahon, T.A., 1998. El Niño/Southern Oscillation and Australian rainfall, streamflow, and drought: links and potential for forecasting. Journal of Hydrology 204, 138–149.

Cho, J., Bosch, D.D., Vellidis, G., Lowrance, R., Strickland, T.C., Submitted for publication. Water quality effects of simulated conservation practice scenarios in the Little River Experimental Watershed, Journal of Soil and Water Conservation.

D'Arrigo, R., Villalba, R., Wiles, G., 2001. Tree-ring estimates of Pacific decadal climate variability. Climate Dynamics 18, 219–224.

Dean, J.D., Snyder, W.M., 1977. Temporally and aerially distributed rainfall. Journal of the Irrigation and Drainage Division: ASCE 103, 221–229.

Einfield, D.B., Mestas-Nunez, A.M., Trimble, P.J., 2001. The Atlantic multi-decadal oscillation and its relation to rainfall and river flows in the continental US. Geophysical Research Letters 28 (10), 2077–2080.

Farge, M., 1992. Wavelet transforms and their applications to turbulence. Annual Review of Fluid Mechanics 24, 395–457.

Feyereisen, G.W., Lowrance, R., Strickland, T.C., Sheridan, J.M., Bosch, D.D., Hubbard, R.K., 2007a. Long-term water chemistry database, Little River Experimental Watershed, southeast coastal plain, United States. Water Resources Research 43. doi:10.1029/2006WR005835.

Feyereisen, G.W., Strickland, T.C., Bosch, D.D., Sullivan, D.G., 2007b. Evaluation of SWAT manual calibration and input parameter sensitivity in the Little River Watershed. Transactions of the ASABE 50 (3), 843–855.

Feyereisen, G.W., Lowrance, R., Strickland, T.C., Bosch, D.D., Sheridan, J.M., 2008. Long-term stream chemistry trends in the southern Georgia Little River Experimental Watershed. Journal of Soil and Water Conservation 63 (6), 475–486.

Grinsted, A., Moore, J.C., Jevrejeva, S., 2004. Application of the cross wavelet transform and wavelet coherence to geophysical time series. Geophysics 11, 561–566.

Gu, D., Philander, S.G.H., 1995. Secular changes of annual and Interannual variability in the Tropics during the past century. Journal of Climate 8, 864–876.

Handler, P., 1990. USA corn yields, the El Niño and agricultural drought: 1867–1988. International Journal of Climatology 10 (8), 819–828.

Hansen, J.W., Irmak, A., Jones, J.W., 1997. El Niño–Southern Oscillation influences on Florida crop yields. Soil and Crop Science Society of Florida 57, 12–16.

Hanson, K., Maul, G.A., 1991. Florida precipitation and the Pacific El Niño, 1895–1989. Florida Scientist 54 (3/4), 160–168.

IPCC, 2007. Climate Change. 2007. Synthesis Report. In: Pachauri, R.K., Reisinger, A., and the Core Writing Team (Eds.), A Contribution of Working Groups I, II, and III to the Fourth Assessment Report of the Intergovernmental Panel on Climate Change. IPCC, Geneva, Switzerland, 104 pp.

Japan Meteorological Agency (JMA), Marine Department, 1991. Climate Charts of Sea Surface Temperatures of the Western North Pacific and the Global Ocean, 51 pp.

Kaplan, A., Cane, M., Kushnir, Y., Clement, A., Blumenthal, M., Rajagopalan, B., 1998. Analyses of global sea surface temperature 1856–1991. Journal of Geophysical Research 103 (18), 567–589.

Keener, V.W., Ingram, K.T., Jacobson, B., Jones, J.W., 2007. Effects of El-Niño/Southern Oscillation on simulated phosphorus loading. Transactions of the ASABE 50 (6), 2081–2089.

Kiladis, G.N., Diaz, H.F., 1989. Global climate anomalies associated with extremes in the Southern Oscillation. Journal of Climate 2 (9), 1069–1090.

Kulkarni, J.R., 2000. Wavelet analysis of the association between the southern oscillation and the Indian summer monsoon. International Journal of Climatology 20, 89–104.

Kwon, H.H., Lall, U., Moon, Y., Khalil, A.F., Ahn, H., 2006. Episodic interannual climate oscillations and their influence on seasonal rainfall in the everglades national park. Water Resources 42.

Labat, D., 2008. Wavelet analysis of the annual discharge records of the world's largest rivers. Advances in Water Resources 31, 109–117.

Lowrance, R.K., Leonard, R.A., Asmussen, L.E., 1985. Nutrient budgets for agricultural watersheds in the southeastern coastal plain. Ecology 66 (1), 287–296.

Lowrance, R., Todd, R.L., Asmussen, L.E., 1984a. Nutrient cycling in an agricultural watershed: streamflow and artificial drainage. Journal of Environmental Quality 13, 27–32.

Lowrance, R., Todd, R., Fail Jr., F., Hendrickson, O., Leonard, R., Asmussen, L.E., 1984b. Riparian forests as nutrient filters in agricultural watersheds. BioScience 34 (6), 374–377.

Pascual, M., Rodo, X., Ellner, S.P., Colwell, R., Bouma, M.J., 2000. Cholera dynamics and El Niño Southern Oscillation. Science 289 (5485), 1766–1769.

Piechota, T.C., Dracup, J.A., 1999. Long-range streamflow forecasting using El Niño–Southern Oscillation indicators. Journal of Hydrologic Engineering 4 (2), 144–151.

Rajagopalan, B., Lall, U., 1998. Interannual variability in western US precipitation. Journal of Hydrology 210, 51–67.

Rasmusson, E.M., Wallace, J.M., 1983. Meteorological aspects of El Niño/Southern Oscillation. Science 222, 1195–1201.

Ropelewski, C.F., Halpert, M.S., 1986. North American precipitation and temperature patterns associated with the El Niño/Southern Oscillation (ENSO). Monthly Weather Review 114, 2352–2362.
Schmidt, N., Lipp, E.K., Rose, J.B., Luther, M., 2001. ENSO influences on seasonal rainfall and river discharge in Florida. Journal of Climate 14 (4), 615–628.
Sheridan, J.M., 1997. Rainfall streamflow relations for coastal plain watersheds. ASAE Applied Engineering in Agriculture 13 (3), 333–344.
Sheridan, J.M., Knisel, W.G., 1989. Rainfall trends in the Georgia Coastal Plain. In: Hatcher, K.J. (Ed.), Proceedings of the 1989 Georgia Water Resources Conference. University of Georgia, Athens, GA, pp. 9–11.
Sheridan, J.M., Yates, P., Asmussen, L.E., 1983. Hydrology and nutrient and sediment movement from Southeastern Coastal Plain watersheds. University of Georgia College of Agricultural Experimental Stations (Spec. Pub. 23).
Sheridan, J.M., Merkel, W.H., Bosch, D.D., 2001. Peak rate factors for flatland watersheds. ASAE Applied Engineering in Agriculture.
Stringfield, V.T., 1966. Artesian water in tertiary limestone in the southeastern states. Geological Survey Professional Paper 517. US Government Printing Office, Washington, DC, 101 pp.
Torrence, C., Compo, G.P., 1998. A practical guide to wavelets analysis. Bulletin of the American Meteorological Society 79 (1), 61–78.
Trenberth, K.E., 1997. The definition of El Niño. Bulletin of the American Meteorological Society 78 (12), 2771–2777.
Wang, B., 1995. Interdecadal changes in El Niño onset in the last four decades. Journal of Climate 8, 267–285.
Wang, Y., Wang, B., 1996. Temporal structure of the Southern Oscillation as revealed by waveform and wavelet analysis. Journal of Climate 9, 1586–1598.
World Meteorological Organization, 1966, Technical Note No. 79: Climatic Change, WMO-No., 195.TP.100, Geneva, 80 pp.
Yates, P., 1976. Design, construction, and operation of streamflow measuring facilities in the Little River Watershed, Georgia. Agricultural Research Service ARS-S 148, USDA-ARS, Washington, DC.